

Research Paper

## Multifunctional Peptide-Conjugated Hybrid Silica Nanoparticles for Photodynamic Therapy and MRI

Hamanou Benachour<sup>1,2</sup>, Aymeric Sève<sup>3</sup>, Thierry Bastogne<sup>1,2,4</sup>, Céline Frochot<sup>3,5</sup>, Régis Vanderesse<sup>6,7</sup>, Jordane Jasniewski<sup>8</sup>, Imen Miladi<sup>9,10</sup>, Claire Billotey<sup>9,10,11</sup>, Olivier Tillement<sup>9,10</sup>, François Lux<sup>9,10</sup>, Muriel Barberi-Heyob<sup>1,2,5,12</sup>✉

1. Université de Lorraine, CRAN, UMR 7039, Campus Sciences, BP 70239, Vandœuvre-lès-Nancy Cedex, 54506, France
2. CNRS, CRAN, UMR 7039, France
3. CNRS, LRGP, UPR 3349, 1 rue Grandville, Nancy, 54000, France
4. Inria, BIGS, France
5. CNRS, GdR 3049 Photomed, France
6. Université de Lorraine, LCPM, UMR 7568, Nancy, 54000, France
7. CNRS, LCPM, UMR 7568, France
8. Université de Lorraine, LIBio, INPL-ENSAIA, 2, avenue de la forêt de Haye, Vandœuvre-lès-Nancy Cedex, 54516, France
9. Université Claude Bernard Lyon 1, LPCML, UMR 5620, Villeurbanne Cedex, 69622, France
10. CNRS, LPCML, UMR 5620, France
11. Hospices Civils de Lyon, Lyon, 69000, France
12. Centre Alexis Vautrin, CRLCC, avenue de Bourgogne, Vandœuvre-lès-Nancy Cedex, 54511, France

✉ Corresponding author: Muriel Barberi-Heyob. CRAN, UMR 7039, CNRS, Université de Lorraine, Centre Alexis Vautrin, Brabois, Avenue de Bourgogne, 54511 Vandœuvre-lès-Nancy Cedex, France. E-mail : m.barberi@nancy.unicancer.fr. Phone: +33 3 83 59 83 76. Fax: +33 3 83 59 83 78

© Ivyspring International Publisher. This is an open-access article distributed under the terms of the Creative Commons License (<http://creativecommons.org/licenses/by-nc-nd/3.0/>). Reproduction is permitted for personal, noncommercial use, provided that the article is in whole, unmodified, and properly cited.

Received: 2012.06.18; Accepted: 2012.08.14; Published: 2012.09.29

### Abstract

Photodynamic therapy (PDT) is an emerging theranostic modality for various cancer as well as non-cancer diseases. Its efficiency is mainly based on a selective accumulation of PDT and imaging agents in tumor tissue. The vascular effect is widely accepted to play a major role in tumor eradication by PDT. To promote this vascular effect, we previously demonstrated the interest of using an active-targeting strategy targeting neuropilin-1 (NRP-1), mainly over-expressed by tumor angiogenic vessels. For an integrated vascular-targeted PDT with magnetic resonance imaging (MRI) of cancer, we developed multifunctional gadolinium-based nanoparticles consisting of a surface-localized tumor vasculature targeting NRP-1 peptide and polysiloxane nanoparticles with gadolinium chelated by DOTA derivatives on the surface and a chlorin as photosensitizer. The nanoparticles were surface-functionalized with hydrophilic DOTA chelates and also used as a scaffold for the targeting peptide grafting. *In vitro* investigations demonstrated the ability of multifunctional nanoparticles to preserve the photophysical properties of the encapsulated photosensitizer and to confer photosensitivity to MDA-MB-231 cancer cells related to photosensitizer concentration and light dose. Using binding test, we revealed the ability of peptide-functionalized nanoparticles to target NRP-1 recombinant protein. Importantly, after intravenous injection of the multifunctional nanoparticles in rats bearing intracranial U87 glioblastoma, a positive MRI contrast enhancement was specifically observed in tumor tissue. Real-time MRI analysis revealed the ability of the targeting peptide to confer specific intratumoral retention of the multifunctional nanoparticles.

Key words: Targeted PDT; neuropilin-1; brain tumor; MRI; functionalized theranostic nanoparticles

## Introduction

Both cancer diagnosis and treatment depend on selective delivery of appropriate agents to the malignant tissues. Photodynamic therapy (PDT) is an increasingly recognized theranostic alternative to treat a variety of cancer diseases. This technique involves the preferential uptake of photosensitizing molecules, also known as photosensitizers, by target tissue followed by localized photoirradiation with visible light at an appropriate wavelength and dosage. Photo-activation of the photosensitizer results in the formation of photosensitizer excited state that transfers its energy to surrounding molecular oxygen to locally generate reactive oxygen species (ROS), such as singlet oxygen ( $^1\text{O}_2$ ), which damage target tumor cells and vasculature inducing tumor cells death [1-3]. Nevertheless, the clinical efficacy of PDT is often limited by the difficulty in systemic administration of mostly hydrophobic photosensitizers. The most commonly used photosensitizing agents are porphyrin-based molecules [4]. Many of them are limited because of poor water solubility, prolonged cutaneous photosensitivity, inadequate pharmacokinetics and low tumor selectivity [5]. To overcome these limitations, numerous approaches have been proposed to direct the photosensitizer to tumor by active targeting strategies, including conjugation to specific antibodies and receptor peptide ligands [6-8], and encapsulation of the photosensitizer within nano-sized carriers, such as emulsions, liposomes, and nanoparticles to enhance their water solubility and deliver higher local concentrations at the tumor tissue [9-11].

In this aim, vascular targeted PDT also appears as a promising targeting approach in cancer treatment that has received considerable attention [12, 13]. Destruction of the vasculature may indirectly lead to tumor eradication, following deprivation of life-sustaining nutrients and oxygen [14, 3], and this vascular effect is thought to play a major role in the destruction of some vascularized tumors by PDT [15, 13, 16]. Therefore, tumor neovasculature known to express specific molecular markers [17] is a potential target of PDT damage. We have previously described the conjugation of a chlorine-type photosensitizer (TPC) to an heptapeptide (ATWLPPR), specific for the vascular endothelial growth factor (VEGF) receptor, neuropilin-1 (NRP-1) [18, 19]. We evidenced the implication of NRP-1 in the cellular incorporation of the conjugate [20], and its *in vitro* efficiency as compared to non-targeted form [19]. *In vivo* evaluation demonstrated the interest of using this active-targeting strategy, allowing efficient and selective accumulation of the conjugated photosensitizer in endothelial cells

of tumor vessels [21, 22]. Although the peptide-conjugated photosensitizer improved the tumor-targeting efficacy, we observed a degradation of the peptide in plasma from 2 h post-intravenous injection and biodistribution findings suggested that its appearance in plasma mainly resulted from the degradation of the peptidic moiety into organs of the reticulo-endothelial system [20, 23].

The use of biocompatible nano-carriers as platforms to deliver photosensitizing and imaging agents has been reported to improve PDT efficiency and cancer detection [24-27]. Nanoparticles not only allow delivering of large amount of PDT and imaging agents, but can also be tailored to an appropriate size for enhancing their passive preferential accumulation in tumor tissue owing to the "enhanced permeability and retention effect" [28]. Due to their surface area, nanoparticles can be functionalized with various functional groups with diverse array of chemical and biochemical properties, including tumor selective ligands for active targeting strategies. We previously reported that hybrid silica-based nanoparticles seem to be very promising delivery systems satisfying all the requirements for an ideal targeted PDT [29, 30]. Among them, hybrid gadolinium oxide nanoparticles have been suggested as very attractive system aiming to combine magnetic resonance imaging (MRI) and treatment [31, 32, 33]. We recently described the synthesis and photophysical characteristics of multifunctional silica-based nanoparticles consisting of a surface-localized tumor vasculature targeting peptide and encapsulated PDT and imaging agents [34]. *In vitro* investigations revealed that peptide-functionalized nanoparticles specifically bound to NRP-1 recombinant protein, and conferred photosensitivity to cells over-expressing this receptor, demonstrating that the photosensitizer covalently grafted within the nanoparticle matrix can be photo activated to induce cytotoxic effects *in vitro* [34]. *In vitro* characterization studies of these nanoparticles revealed a photodynamic efficiency in a concentration-dependent manner, providing direct evidence that the conjugated photosensitizer in the nanoparticle matrix could be photoactivated to yield cytotoxic reactive oxygen species.

In the present study, we described the development and the *in vitro* and *in vivo* evaluation of novel multifunctional nanoplatfoms consisting of a surface-localized tumor vasculature targeting NRP-1 and encapsulated PDT and imaging agents, as potential theranostic system for PDT and imaging of cancer. We optimized peptide-targeted silica-based small nanoparticles grafted by gadolinium chelates for MRI and a chlorin as a photosensitizer. Multifunctional nano-

particles were evaluated *in vitro*, demonstrating an efficient photodynamic activity on cancer cells, related to the photosensitizer concentration and light dose, and their ability to target NRP-1 recombinant protein. *In vivo* studies on rats bearing an orthotopic human brain tumor (U87) revealed a tumoritropic accumulation of the multifunctional nanoparticles, providing a tumor positive MRI contrast enhancement and highlighted the role of the peptide-targeted nanoparticle in the intratumoral retention of the nanoparticles.

## Materials and Methods

### Nanoparticles synthesis and functionalization

The approach developed is based on multifunctional silica-based nanoparticles consisting of a surface-localized tumor vasculature targeting NRP-1 peptide and gadolinium chelates as MRI contrast agent and encapsulated a chlorin as photosensitizer. Multifunctional silica-based nanoparticles were designed, consisting of a surface grafted tumor targeting peptide H-Ala-Thr-Trp-Leu-Pro-Pro-Arg-OH (called ATWLPPR) and encapsulated a photosensitizer (a chlorin, (5-(4-carboxyphenyl)-10,15,20-triphenylchlorin, TPC) and a MRI contrast agent (gadolinium DOTAGA), and noted NP-TPC-ATWLPPR. Nanoparticles without photosensitizer and surface targeting peptide were also synthesized and considered as control, noted NP. The synthesis of Gd<sub>2</sub>O<sub>3</sub> nanoparticles embedded in a polysiloxane shell has been widely described previously by our group [35-37, 32]. The top down process leading from the gadolinium oxide particles to the ultrasmall polysiloxane particles with gadolinium chelates at the surface has been recently published [33].

**Preparation of gadolinium oxide core:** Gadolinium chloride salt (3.346 g, GdCl<sub>3</sub>·6H<sub>2</sub>O) was placed in 60 mL of diethylene glycol (DEG) at room temperature under vigorous stirring. The suspension was heated at 140°C until the total dissolution of gadolinium chloride salt (about 1 h). When the solution was clear, 0.3 equivalent volume of sodium hydroxide solution (1.33 mL, 2.03 M) was added drop by drop under vigorous stirring. Afterwards, the solution was heated and stirred at 180°C for 3 h. A transparent colloid of gadolinium oxide nanoparticles was obtained and brought back to room temperature before storage at -18°C.

**Peptide synthesis:** The synthesis of H-AT(tBu)W(Boc)LPPR(Pbf)-OH peptide, called protected ATWLPPR, was carried out on a fully automated ResPepXL synthesizer (Intavis AG, Köln, Germany) according to a classical 9-fluorenyl-methoxy-carbonyl (Fmoc)/tBu sol-

id-phase methodology. Details of the method were previously described by our group [38, 34].

**Photosensitizer synthesis:** 5-(4-carboxyphenyl)-10,15,20-triphenylchlorin (TPC) was synthesized as described by Whitlock [39] and our group [40] as well as 5,10,15,tri-(p-tolyl)-20-(p-carboxylphenyl)chlorin-succinidyl ester (TPC-NHS).

**Grafting of TPC-NHS into polysiloxane shell and coating of gadolinium oxide cores by the grafted polysiloxane shell:** A solution containing TPC-NHS (26.4 μmol) and two equivalents of aminopropyltriethoxysilane (APTES, 52.8 μmol) dissolved in 2.5 mL of dimethylsulfoxide (DMSO) was prepared as a precursor TPC-APTES and stirred for 2 h at room temperature. The silane precursors (APTES (0.75 mL) and triethoxy silane (TEOS, 0.5 mL)) and hydrolysis solution (aqueous Et<sub>3</sub>N in DEG (1.07 M of triethylamine (TEA), 0.75 M of water)) were sequentially and alternatively added to 60 mL DEG solution containing Gd<sub>2</sub>O<sub>3</sub> nanoparticles ([Gd]=45 mM) under stirring at 40°C. The whole addition of silane precursors and hydrolysis solution is performed in 4 steps. Each step consists in the addition to the colloid of a portion of the silane precursors mixture (25% for each step) followed by the addition of hydrolysis solution mixture (25% for each step). The solution of TPC-APTES is added in the first step with the other silane precursors. The delay between both additions is 24 h. After the last addition, the final mixture was stirred for 48 h at 40°C.

**Functionalization of the polysiloxane shell by DOTAGA:** To facilitate the dispersion of the particles in biological media in one hand, and to provide chemical functions allowing further functionalization of the nanoparticles (i.e. with targeting peptide) in the other hand, DOTAGA chelate (1,4,7,10-tetraazacyclododecane-1-glutaric anhydride-4,7,10-triacetic) acid was covalently grafted at the surface of the polysiloxane shell. DOTAGA is coupled to the nanoparticles through an amide link by the reaction with the amine functions of the APTES. DOTAGA (1.47 g, DOTAGA/APTES ratio is 1.0) in 6 mL of anhydrous DMSO is added to 60 mL of the precedent colloidal solution and stirred for 1 h. DOTAGA was furnished by Chematech (France).

**Covalent grafting of the protected peptide on DOTA-nanoparticles:** To prepare the nanoparticles grafted with peptide, 1.64 × 10<sup>-8</sup> mol of gadolinium in DOTA-nanoparticles was dispersed in 7 mL of water/dimethylsulfoxide (DMSO), 1/1, v/v. The DOTA carboxylic acid functions were first activated by 5 equivalents of a mixture EDC/HBTU, 1/1, (EDC, 8.2 × 10<sup>-8</sup> mol, 16 μg, HBTU 8.2 × 10<sup>-8</sup> mol, 32 μg, DIEA 10 μL). The mixture was stirred during 10 min before

addition of 122.8  $\mu\text{g}$  ( $9.84 \times 10^{-8}$  mol) protected peptide ATWLPPR. After 18 h at room temperature under stirring, water and DMSO were evaporated and 5 mL of pure trifluoroacetic acid (TFA) was added to deprotect the side chains of the peptide. The stirring was carried on during 2 h at room temperature. Ultrapure water was added and the solvents were evaporated. Several cycles of addition of water and evaporation were realized to eliminate most of TFA and DMSO. The purification of the peptide-functionalized nanoparticles was realized first by dialyses with a 5000 Da cellulose membrane against ultrapure water, secondly by several cycles of dialysis during 2 h or 3 h each followed by ultrafiltrations with Vivaspin® (MCWO 5000 Da) during 7 min at 3500 g. Finally, the water was removed under vacuum and the concentration of the nanoparticles was adjusted. Thanks to the fluorescence of the tryptophan residue (excitation and emission wavelengths at 280 and 350 nm, respectively); it was possible to estimate the number of grafted peptide onto the nanoparticles. The number of the peptide units coupled to the nanoparticles has been estimated by comparing the fluorescence of the tryptophan of the peptide coupled to the nanoparticle to a fluorescence calibration curve of the peptide in solution.

### Photon Correlation Spectroscopy (PCS) and zeta potential measurements

PCS and Zeta potential measurements were performed with a Zetasizer Nano ZS (Malvern, England) equipped with a 532 nm frequency doubled DPSS laser, a measurement cell, a photomultiplier and a correlator. Scattering intensity was measured at a scattering angle of  $173^\circ$  relative to the source using an avalanche of photodiode detector. Prior to analysis, nanoparticles were suspended in ultrapure water and adjusted to pH  $\sim 7.0$ . 1 ml of nanoparticles sample at 5 mM of gadolinium was measured in a clear disposable Zeta cell (DTS1060 Malvern). The measurements were made at a position of 5.50 mm and 2.00 mm from the cuvette wall for the PCS or Zeta potential measurements, respectively, with an automatic attenuator and at a controlled temperature of  $20^\circ\text{C}$ . This setup allows considerable reduction of the signal due to multiple scattering events and enables working in slightly turbid media. Intensity autocorrelation functions were analysed by CONTIN algorithm in order to determine the distribution of translational  $z$ -averaged diffusion coefficient of particles,  $D_T$  ( $\text{m}^2 \cdot \text{s}^{-1}$ ). The  $D_T$  parameter is related to the hydrodynamic radius ( $R_h$ ) of particles through the Stokes-Einstein relationship:

$$D_T = k_B T / 6\pi\eta R_h$$

where  $\eta$  is the solvent viscosity (Pa.s),  $k_B$  is the Boltzmann constant ( $1.38 \times 10^{-23}$  N.m.K $^{-1}$ ),  $T$  is the absolute temperature ( $^\circ\text{K}$ ) and  $R_h$  (m) is the equivalent hydrodynamic radius of a sphere having the same diffusion coefficient than the particles [41]. For each sample, 15 runs of 10 s were performed with three repetitions.

### Photophysical properties

Absorption spectra were recorded on a Perkin-Elmer (Lambda 35, Courtaboeuf, France) UV-visible spectrophotometer. Fluorescence spectrum were recorded on a SPEX Fluorolog-3 spectrofluorimeter (Jobin Yvon, Longjumeau, France) equipped with a thermo stated cell compartment ( $25^\circ\text{C}$ ), using a 450 W Xenon lamp. The spectra were performed on suspensions of samples (nanoparticles and free TPC) prepared in ethanol.

### Binding of functionalized nanoparticles to recombinant NRP-1 protein

A competitive binding assay was used. Neuro-pilin-1 was obtained from R&D Systems (Lille, France), as recombinant chimeric protein. The surface of Maxisorp microplates (Dutscher) was coated with NRP-1 (2  $\mu\text{g}/\text{mL}$ ) in phosphate buffered saline (PBS) overnight at room temperature. After washing (PBS containing 0.05% Tween 20), the plates were blocked with PBS containing 0.5% bovine serum albumine (BSA, blocking buffer) during 1h at  $37^\circ\text{C}$ , to prevent non-specific interactions. Binding of the functionalized nanoparticles to NRP-1 was assessed using 5 ng/mL of biotinylated VEGF $_{165}$  (R&D Systems) in blocking buffer containing 2  $\mu\text{g}/\text{mL}$  heparin. Biotinylated VEGF $_{165}$  was added to the coated wells in the absence or presence of increasing concentrations of NP-TPC-ATWLPPR or control NP as competitors, or large excess of unlabelled VEGF $_{165}$  as positive control (0.5  $\mu\text{g}/\text{mL}$ , R&D Systems). After a 2 h-incubation at room temperature, the wells were washed and the amount of bound biotinylated VEGF $_{165}$  was stained with streptavidin horseradish peroxidase conjugate (R&D Systems) for 20 min at room temperature. Following a wash to remove unbound enzyme conjugate, a substrate solution (R&D Systems) was added. After 30 min at room temperature, reaction was stopped by the addition of Stop Solution (R&D Systems) and optical densities were measured at 450 nm against a background control containing only blocking buffer, using a Multiskan microplate reader (Labsystem, Cergy-Pontoise, France). Results were expressed as relative absorbance to negative control without any competitor. Reported values are the average of triplicate measurements.

## Cell line and culture

To investigate the potential of functionalized nanoparticles to induce *in vitro* photodynamic effect on tumor cells, MDA-MB-231 human breast cancer cells over-expressing the vascular neuropilin-1 (NRP-1) receptor were used. MDA-MB-231 cells were purchased from American Type Culture Collection (ATCC, Manassas, VA, USA). Cells were routinely grown in Roswell Park Memorial Institute (RPMI 1664) medium (Invitrogen, France) supplemented with 9% heat-inactivated fetal bovine serum (PAN<sup>TM</sup> Biotech GmbH, Germany), 100 U/mL penicillin and 100 µg/mL streptomycin (Invitrogen, France), and 2 mM L-Glutamine (Invitrogen, France) in a controlled atmosphere of 5% CO<sub>2</sub>, 95% humidified air at 37°C in 75 cm<sup>2</sup> culture flasks. Cell culture materials were purchased from Costar (Dutscher, Brumath, France).

## In vitro cytotoxicity and photodynamic activity

*In vitro* cytotoxicity and photo-induced cytotoxicity of the synthesized nanoparticles were investigated using the metabolic-based cell viability assay (MTT) and the real-time impedance-based analysis.

**Real-time impedance-based cell analysis:** MDA-MB-231 cells attachment, proliferation and size variations were monitored in real-time and measured as impedance using 96-well E-Plates<sup>TM</sup> and the xCELLigence system (Real Time Cell Analyzer Single Plate (RTCA SP<sup>®</sup>) system). The xCELLigence system was developed to monitor cell proliferation in real-time, without incorporation of dyes, by measuring electrical impedance created by cells across the high-density electrode array coating the bottom of the wells [42]. Impedance value is automatically converted to Cell Index (CI) value that is defined as relative change in electrical impedance, created by attached cells, to represent cell status, and is directly proportional to number, size, and attachment forces of the cells.

Background impedance of the E-Plate was first determined before seeding the cells by the addition of 50 µL culture medium to each well, and subtracted automatically by the RTCA software following the equation:  $CI = (Z_i - Z_0) / 15$  with  $Z_i$  as the impedance at any given time point and  $Z_0$  as the background signal [43]. Subsequently, a 150 µL cell suspension containing 10<sup>4</sup> MDA-MB-231 cells was seeded in each well, and allowed to settle at the bottom of wells for 20 min before starting impedance measurement in 15 min intervals. 24 h after seeding, 10 µL of growth medium without or with increasing final concentrations of photosensitizer (0.05, 0.10, 0.50, 1.00 or 10.00 µM) in NP-TPC-ATWLPPR or the corresponding final concentrations of gadolinium (2.9, 5.8, 29.2, 58.5 or 585.0

µM) for the control NP was added in each well, and the cultures were kept in darkness. Each concentration was tested in sixuplicate. To allow nanoparticles internalization, the cells were grown for further 24 h during which impedance was measured every 15 min. The cells were then washed three times with growth medium and the medium was renewed by 150 µL fresh growth medium. The cell growth was then monitored for the indicated time, and impedance was measured every 15 min. Before, cells were either exposed to various doses of light (1, 5, or 10 J/cm<sup>2</sup>) using a diode laser, Ceralas PDT 652 (CeramOptec GmbH, biolitec, Germany) to assess the photo-induced cytotoxicity of the NP-TPC-ATWLPPR, or let without irradiation to determine their cytotoxicity in darkness. Irradiation was carried out at 652 nm with an irradiance of 4.54 mW/cm<sup>2</sup>. Based on impedance measurements, cell index values were automatically derived and recorded as a function of time from the time of plating until the end of the experiments.

**MTT assay:** Cell proliferation and survival after incubation with various concentrations of nanoparticles without or with light irradiation was also measured using a single-point metabolic-based assay; 3-(4,5-dimethylthiazol-2-yl)-2,5-diphenyl tetrazolium bromide (MTT). Briefly, MDA-MB-231 cells were plated in sixuplicate at a density of 4 × 10<sup>3</sup> cells per well in 96-well flat-bottomed microtiter plates in the volume of 200 µL per well, and let to adhere in 5% CO<sub>2</sub> at 37°C. Forty-eight hours after plating, wells were emptied and 200 µL of fresh medium without or with nanoparticles at the indicated concentrations of photosensitizer (in NP-TPC-ATWLPPR) or the corresponding concentrations of gadolinium for the control NP without TPC and without peptide (NP) was added in each well. After a 24 h-incubation at 37°C, the medium was removed and cells were washed three times with fresh medium, and 150 µL of medium were added. The cells were then either exposed to various doses of light (1, 5, or 10 J/cm<sup>2</sup>) using a diode laser, Ceralas PDT 652 (CeramOptec GmbH, biolitec, Germany) to assess the photodynamic activity of the nanoparticles, or let without irradiation to determine their cytotoxicity in darkness. Following a further 24h-incubation at 37°C, cell survival was then measured as described previously [44]. Cell viability was expressed as the percentage of the controls cultivated under the same conditions without nanoparticles exposure.

## Animals and tumor xenograft model

Male athymic nude rats (mean weight 100 g, rnu/rnu, homozygous) purchased from Harlan (Harlan, Gannat, France) were used in the present

study. Animal care and studies were performed according to the guidelines of the French Government (degree 87-848 of October 19, 1987) and approved by our institutional agreement number (C 54-547-03). Rats were housed in an isolation facility at 25°C and fed a standard pellet diet and provided water *ad libitum*. U87 human glioblastoma cells were stereotactically implanted into the right brain hemisphere. For tumor implantation, rats (8 week-old, 180-200g weight at the time of implantation) were anesthetized by an intraperitoneal (*i.p.*) injection of a mixture of ketamine/xylazine (90/10 mg/kg respectively) and immobilized in a Kopf stereotactic frame (900M Kopf Instruments, Tujunga, CA). Following a local anesthesia with Xylocain (AstraZeneca, France) and antiseptic preparation of the head, a midline incision was done and a burr hole was made in the right striatum (coordinates with regard to *bregma*: 0.5 mm anterior and 2.7 mm lateral). U87 cells were washed once with PBS (1x), trypsinized, centrifuged and resuspended at  $5.10^5$  cells/5  $\mu$ L Hank's Buffered Salt Solution (HBSS, 1X). A volume of 5  $\mu$ L of cell suspension was slowly injected at a depth of 4.4 mm into the right caudal-putamen of the animal brain using a 10 $\mu$ L-Hamilton microsyringe coupled in the infusion pump (0.5  $\mu$ L/min). After injection the burr hole was closed with bone wax, the scalp incision sutured with 6.0 Prolene suture and the surface was antiseptically cleaned.

### Nanoparticles preparation and intravenous administration

Nanoparticles were suspended in ultrapure water and NaCl 9‰ (1:1) to obtain a concentration of 100 mM Gd in iso-osmolar solution, pH ~ 7.4. The injection solution was prepared for each type of studied nanoparticles (NP-TPC-ATWLPPR or NP) by dilution in 9‰ NaCl to obtain an injection volume of 500  $\mu$ L (*e.g.* 25  $\mu$ mol of Gd for a body weight of ~ 250 g). The anesthetized rat was catheterized into the caudal vein using a microperfusor (BD Vacutainer Safety-Lok: 23G x 3/4"x7" 0.6x19 mm x178 mm, France). The catheter was filled beforehand with 10% heparin (Heparin 25000 UI), which made it possible to check the venous return, the permeability of the catheter and to prevent its occlusion by coagulated blood. 500  $\mu$ L of the nanoparticles solution, followed by 500  $\mu$ L of 9‰ NaCl to flush the cannula line were slowly injected (during 1 min).

### In vivo magnetic resonance imaging (MRI)

Magnetic resonance imaging of the rat brain was performed by using a 7-Tesla horizontal bore system (Biospec; Brüker, Ettlingen, Germany) equipped with

400 mT/m gradient set and a 30-mm-diameter surface coil for signal reception. Twenty days after intracranial tumor inoculation, the animal was anesthetized with a mixture of air and 4% isoflurane. Anesthesia was maintained throughout the imaging procedure with 1.5-2% isoflurane. The caudal vein was catheterized and the anesthetized animal was immediately prepared for MRI. The rat head was fixed with ear plugs and bar tooth to prevent head movement during acquisition, and respiration was continuously monitored throughout acquisition using a pressure sensitive probe positioned over the rat's diaphragm. Cerebral T2-weighted TurboRARE (Rapid Acquisition with Relaxation Enhancement) spin echo sequences (4200/12 [repetition time msec/echo time msec], 0.651 mm section thickness, 2x2 cm field of view, 512-192 matrix) were acquired for solid tumor location and size estimation. To assess the kinetics of the nanoparticles in the tumor as well as the nanoparticles-enhanced MRI signal intensity, a dynamic T1-weighted flash sequences (86/3.6 [repetition time msec/echo time msec], 0.651 mm section thickness, 2x2 cm field of view, 512-192 matrix) were acquired just before injection and during 60 minutes. Following MRI analysis, rats were sacrificed and right and left hemispheres as well as other organs/tissues were dissected out and kept at -80°C for analysis of gadolinium-based hybrid nanoparticles uptake.

### Inductively coupled plasma-mass spectrometry (ICP-MS) analysis

A Varian 820 MS instrument (Varian, Les Ulis, France) was used to perform ICP-MS (Inductively Coupled Plasma-Mass Spectrometry) analyses in order to evaluate biodistribution of gadolinium hybrid nanoparticles. All samples (organs and urine), dissected out from the rats bearing brain tumor, were completely dissolved with 70% HNO<sub>3</sub> (5 mL per sample) and heated at 90°C until total mineralization. Each mineralized sample was solubilised in 25 mL of milli-Q water (resistivity > 18.2 M $\Omega$ ) and analyzed by ICP-MS (Laboratoire Environnement-Hygiène of Eurofins ASCAL, Forbach, France). The ICP-MS instrument was initialized, optimized and standardized according to manufacturer recommendations.

## Results

### Synthesis and characterization of nanoparticles

Multifunctional small nanoparticles were successfully developed consisting of a gadolinium oxide core as MRI contrast agent, which is coated by a silica shell containing the covalently encapsulated TPC

photosensitizer. The nanoparticles were surface-functionalized with DOTA as hydrophilic chelates and ATWLPPR heptapeptide as a tumor vasculature targeting NRP-1 unit. To evaluate the PDT efficiency and targeting ability of the functionalized nanoparticles, two nanoparticles batches were tested without (NP) or with (NP-TPC-ATWLPPR) TPC photosensitizer and ATWLPPR targeting peptide units.

Size distribution and Zeta potential of the nanoparticles were presented in **Fig. 1A** and **B**, respectively, and values were summarized in **Table 1**. Hydrodynamic diameter was 4.6 and 3.3 nm for NP-TPC-ATWLPPR and NP, respectively. Hence, one can observe that peptide grafting on the surface of nanoparticles (~3 peptides per nanoparticle) and TPC encapsulating into the silica shell (~1.7 TPC molecules per nanoparticle) induce only slight increase in the hydrodynamic diameter (4.6 *vs.* 3.3 nm for NP-TPC-ATWLPPR and NP, respectively). The two nanoparticles batches were characterized by a single narrow peak with around 99.5% of the size distribution by volume (**Fig. 1A**). This indicates that the nanoparticles were monodisperse in water probably because of their derivatization by the DOTA polymers. Zeta potentials were also determined in ultrapure water to avoid the presence of counterions which could neutralize the charges on the nanoparticles. Positive charge of  $12.9 \pm 4.0$  and  $4.3 \pm 3.5$  mV was measured for NP-TPC-ATWLPPR and NP, respectively (**Fig. 1B** and **Table 1**). As suggested by our group [34], the higher positive charge of the peptide-conjugated nanoparticles ( $12.9 \pm 4.0$  mV) may be brought by the surface-grafted peptide ATWLPPR (~3 peptides per nanoparticle). UV/Vis spectra of the NP-TPC-ATWLPPR nanoparticles showed that the nanoparticles displayed similar absorption features to free TPC, with the Soret-band and the respective Q-bands (**Fig. 1C**). No shift of the maximum absorption at Soret-band can be observed, suggesting that the photosensitizer was mainly in a monomeric form without aggregation inside the nanoparticles. This indicates that the photophysical properties of TPC molecules in the nanoparticles were well retained. According to the calibration curve of the UV/Vis absorption spectra of free TPC, the amount of grafted TPC within the nanoparticles NP-TPC-ATWLPPR was estimated around 1.7 TPC molecules per nanoparticle. According to the calibration curve of the fluorescence spectra of free peptide and the fluorescence of the peptide coupled to the nanoparticles in solution, we quantified ~3 peptides per nanoparticle.

**Table 1.** Size and zeta potential of nanoparticles

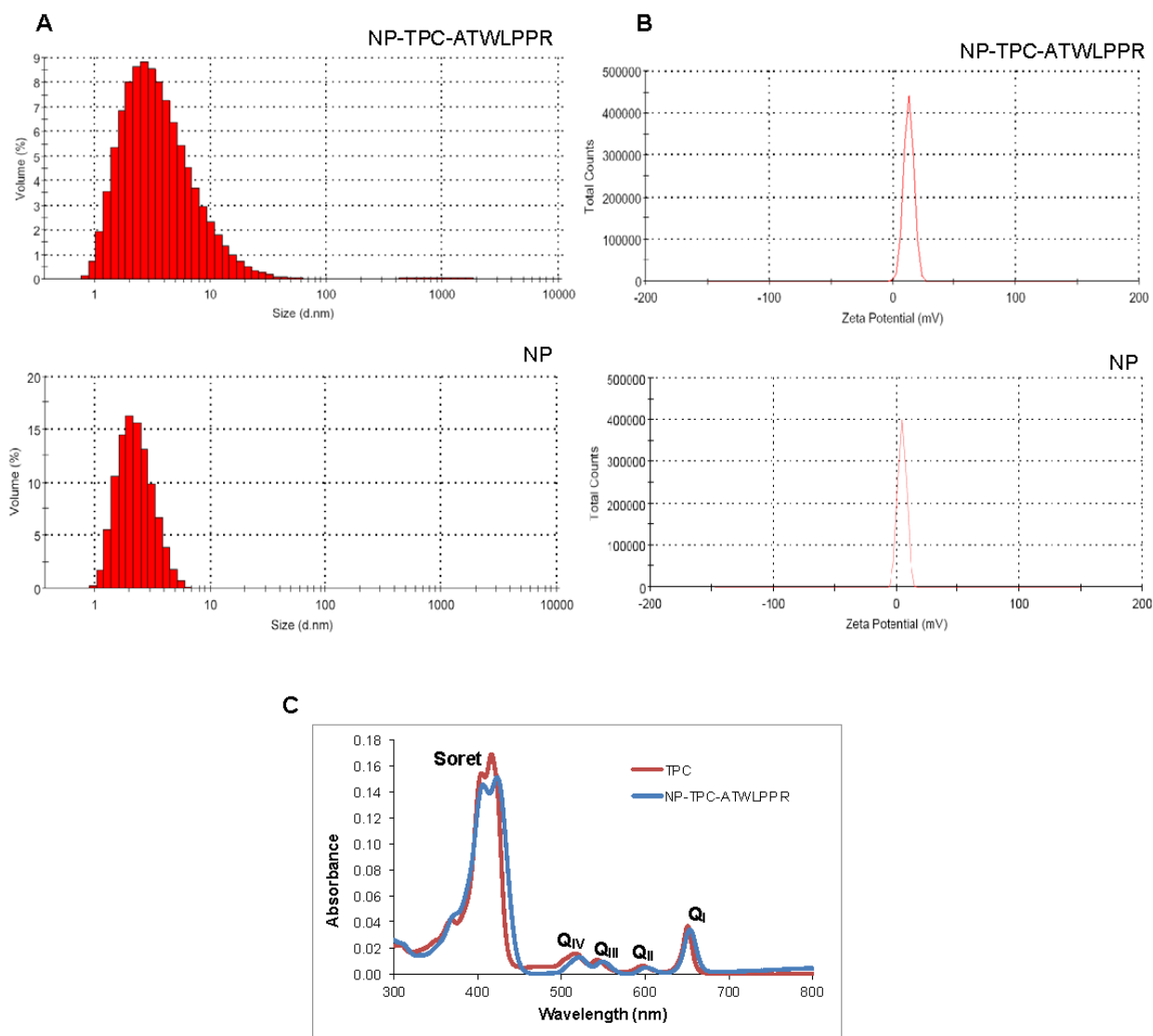
Nanoparticles types	NP-TPC-ATWLPPR	NP
Hydrodynamic diameter (nm)	4.6±3.8	3.3±1.1
Zeta potential (mV)	12.9±4	4.3±3.5

### Molecular affinity of peptide-conjugated nanoparticles

The endothelium-homing peptide ATWLPPR was described to selectively target NRP-1 receptor expressed in angiogenic vasculature [19, 20, 22]. The molecular affinity of the nanoparticles for recombinant NRP-1 protein was evaluated using competitive binding test. Increasing concentrations of peptide conjugated to NP-TPC-ATWLPPR nanoparticles or the corresponding concentrations of gadolinium in the control NP were tested. Results of binding test were presented in **Fig. 2**. Biotinylated VEGF<sub>165</sub> bound to NRP-1 was greatly displaced by the peptide-conjugated nanoparticles NP-TPC-ATWLPPR, indicating that the conjugated nanoparticles bound to recombinant NRP-1 chimeric protein. Although slight interaction of the un-conjugated NP was only detected with the higher concentration tested, ATWLPPR-conjugated nanoparticles showed a peptide concentration-dependent binding to recombinant NRP-1 protein ( $EC_{50} = 56.6 \mu\text{M}$  for NP-TPC-ATWLPPR, corresponding to the concentration of competitor that displaced 50% of VEGF<sub>165</sub> binding).

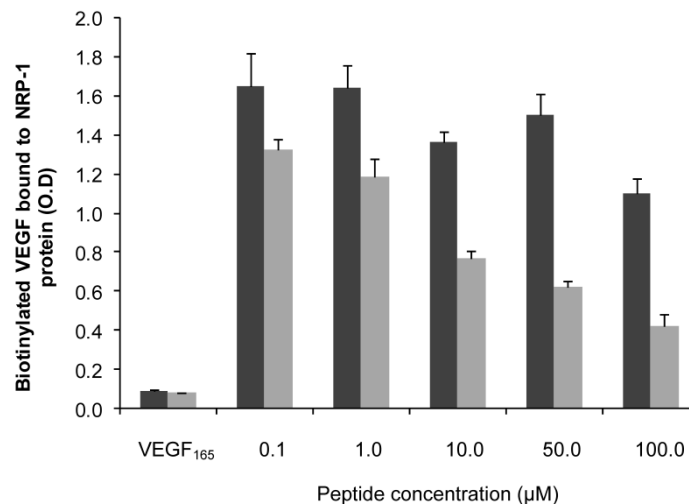
### Nanoparticles-induced dark cytotoxicity *in vitro*

Dark cytotoxicity (without light irradiation) was first assessed by MTT test on the MDA-MB-231 breast cancer cells, overexpressing NRP-1 receptor [38]. Increasing concentrations of nanoparticles-grafted photosensitizer molecules (NP-TPC-ATWLPPR) or photosensitizer-free nanoparticles (NP) (from 0.05 to 10.00  $\mu\text{M}$  of TPC, corresponding to 2.9 to 585.0  $\mu\text{M}$  of gadolinium oxide, respectively) were tested (**Fig. 3**). As shown on **Figure 3A**, 48 h after nanoparticles exposure, cytotoxic effect was evidenced only with the higher concentration (10.00  $\mu\text{M}$ /585.0  $\mu\text{M}$ ) leading to a reduction of 37% and 41% of cell survival for NP-TPC-ATWLPPR and NP, respectively. No cytotoxic effect was measured (mean cell viability superior to 80%) for cells exposed with concentrations from 0.05 to 1.00  $\mu\text{M}$  for both nanoparticle groups (NP-TPC-ATWLPPR and NP) compared to untreated cells (**Fig. 3A**).



**Figure 1.** Absorption spectra, size and zeta potential of gadolinium-based hybrid silica nanoparticles. (A) Size distribution by volume of the hydrodynamic diameter (expressed in nm) of nanoparticles (NP-TPC-ATWLPPR or NP) in suspension at 20°C. (B) Zeta potential distribution (expressed in mV) of the nanoparticles (NP-TPC-ATWLPPR or NP) suspensions. (C) Absorption spectra of free photosensitizer TPC and suspension of NP-TPC-ATWLPPR nanoparticles in ethanol.

**Figure 2.** Binding of ATWLPPR-targeted (NP-TPC-ATWLPPR) and untargeted (NP) nanoparticles to NRP-1 recombinant protein. Binding of the biotinylated VEGF (5 ng/mL) to recombinant chimeric NRP-1 protein, in the presence of 2 µg/mL heparin, was evaluated in competition with an excess of VEGF<sub>165</sub> as positive control (0.5 µg/mL), NP-TPC-ATWLPPR (grey) or NP control (black) at the indicated concentrations of ATWLPPR or the corresponding concentrations of gadolinium (Gd), respectively. Data points show the mean ± S.D., n=3. EC<sub>50</sub> = 56.6 µM (NP-TPC-ATWLPPR)



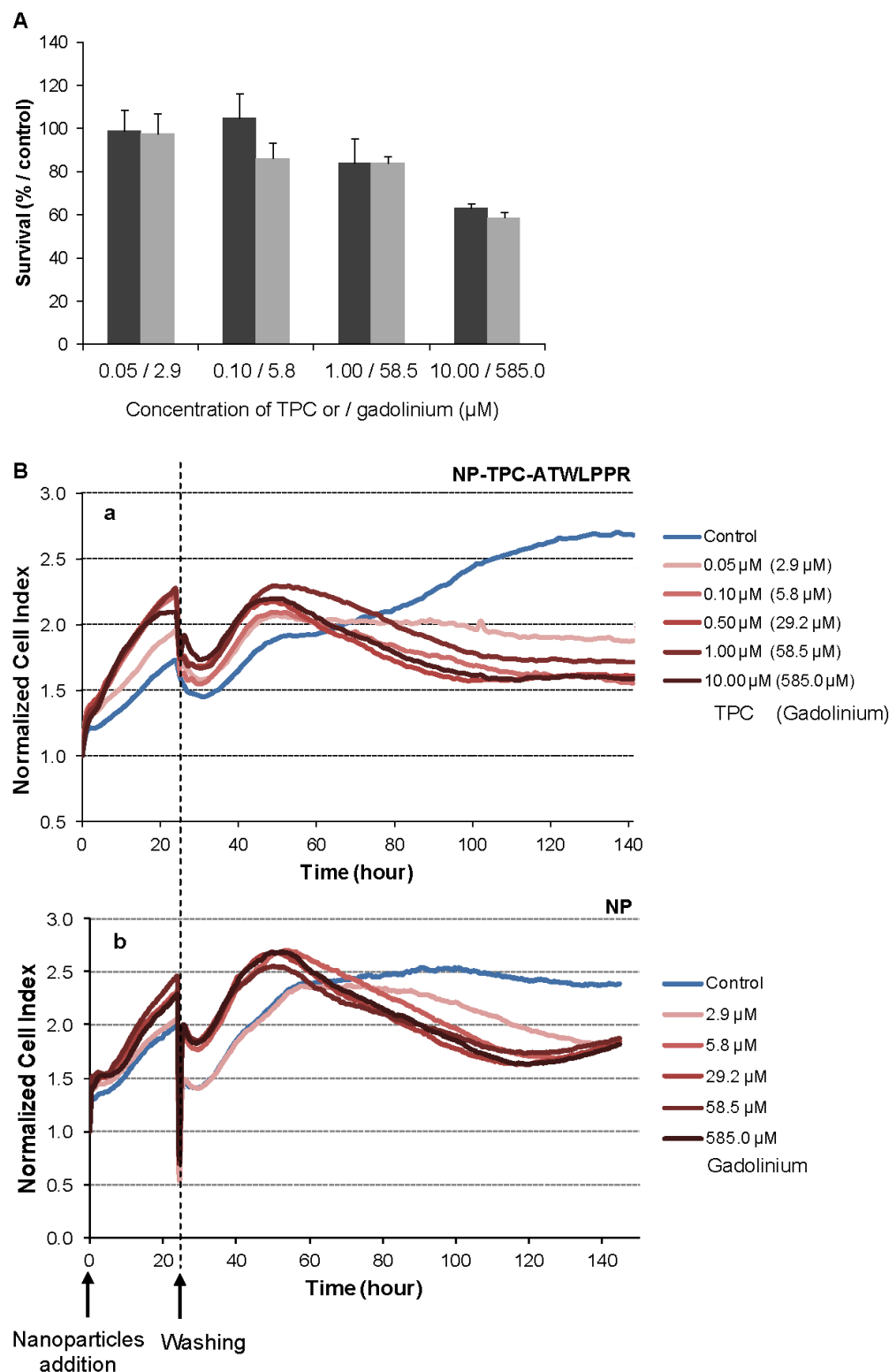


**Figure 3.** Impact of nanoparticles-containing photosensitizer and peptide (NP-TPC-ATWLPPR) or nanoparticles only (NP) on MDA-MB-231 cell activities in darkness. A) MDA-MB-231 cells were exposed to NP-TPC-ATWLPPR (black) or NP (gray) at the indicated concentrations for 24 h at 37°C. Cells were washed and incubated at 37°C for further 24 h. Cell viability was then measured using MTT test (values are presented as the mean ± S.D). B) Kinetics of the normalized cell index of the MDA-MB-231 cells exposed to various concentrations of NP-TPC-ATWLPPR (a) or the corresponding concentrations of gadolinium in the control NP (b) for 24h before washing. Cell index was monitored during 143 h after nanoparticles exposure by using the xCELLigence system. All reported data are the means of six replicates.

We also used a real-time cell analysis system to investigate the dynamics of cytotoxic effects of multifunctional ultrasmall nanoparticles. RTCA system measures impedance-based signals and provides dynamic information about cell response. The cellular response was continually monitored for 143 h in darkness from the time of nanoparticles addition. As shown in **Figure 3B**, electrical impedance measurements from adherent cells, expressed as normalized cell index kinetics, showed no decrease in cell index values whatever the nanoparticles type (NP and NP-TPC-ATWLPPR) concentration used as compared to untreated cells. A transient decrease of cell index was recorded at 24 h-post addition, related to the temporary interruption of impedance measurement during the washing step performed to washing off the un-internalized nanoparticles. However, from ~ 60 h after nanoparticles exposure, cell index kinetics were clearly modified displaying an evident time-dependent decrease of cell index for all the concentrations tested, suggesting a late cellular effect on cell proliferation.

### **In vitro photodynamic activity of nanoparticles**

On the basis of the data obtained from the dark cytotoxicity studies using MTT test (**Fig. 3A**), photodynamic activity was investigated with two non cytotoxic concentrations of TPC (0.1 and 1.0  $\mu\text{M}$ ) into the nanoparticles NP-TPC-ATWLPPR. MDA-MB-231 cancer cells were exposed to 0.1 and 1.0  $\mu\text{M}$  of TPC into NP-TPC-ATWLPPR for 24 h. Following washing, the cells were irradiated with various doses of red light (652 nm). After 24 h post-irradiation, cell viability was estimated with MTT test. As shown in **figure 4**, the nanoparticles induced a light dose-dependent increase in photocytotoxicity, achieving at 20  $\text{J}/\text{cm}^2$  a

decrease in cell viability up to 24 and 1% for 0.1 and 1.0  $\mu\text{M}$  TPC, respectively. Moreover, the nanoparticles exhibited photocytotoxicity in a TPC concentration-dependent manner as the nanoparticles at 1.0  $\mu\text{M}$  was 3.3 times more effective than 0.1  $\mu\text{M}$  (50% cell growth inhibitory light dose,  $\text{DL}_{50} = 9.16$  vs. 2.80  $\text{J}/\text{cm}^2$  at 0.1 and 1.0  $\mu\text{M}$ , respectively).

The dynamic response of the MDA-MB-231 cancer cells exposed to increasing concentrations of NP-TPC-ATWLPPR and various doses of light was also monitored using real-time impedance-based analysis (**Fig. 5A-B-C**). As expected according to our findings from dark cytotoxicity kinetics (**Fig. 3B**), no decrease in cell index values was observed during the first 24 h post-exposure to nanoparticles before light irradiation (**Fig. 5, left panel**). However, cell index kinetics obtained during the time interval from 25 to 55 h post-irradiation clearly showed discriminant profiles (**Fig. 5A-B-C, right panel**). According to nanoparticles concentrations and light doses, kinetic profiles showed a transient or a persistent decrease of normalized cell index (**Fig. 5A-B-C, right panel**). Beside the nanoparticles concentration- and the light dose-dependent photocytotoxicity, distinct phases of cell response along the post-irradiation period can be highlighted, thus showing time-dependent cellular effect. Interestingly, as shown on **Fig. 5-D (right panel)**, photosensitizer-free nanoparticles (NP) showed no decrease of cell index values whatever the concentrations even after light irradiation with 10  $\text{J}/\text{cm}^2$  as compared to untreated cells. This means that the nanoparticles-induced photocytotoxicity relies on the photoactivation of the photosensitizer molecules grafted inside the nanoparticles.

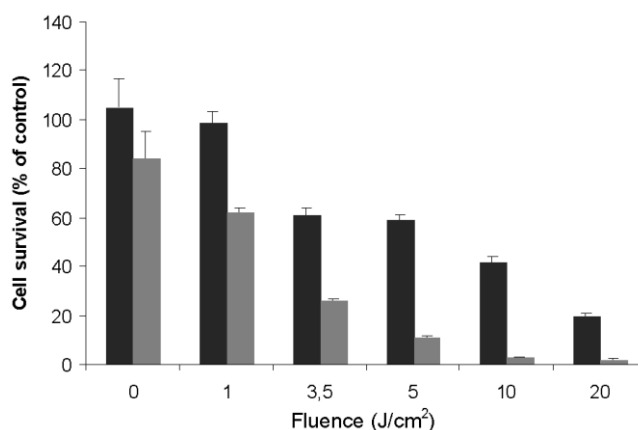


**Figure 4.** *In vitro* photodynamic activity of nanoparticles-containing photosensitizer and peptide (NP-TPC-ATWLPPR) according to MTT assay. MDA-MB-231 cells were exposed to 0.1  $\mu\text{M}$  (black) and 1.0  $\mu\text{M}$  (gray) of TPC in NP-TPC-ATWLPPR. Following a 24 h-incubation at 37°C, cells were washed and exposed to the indicated doses of light and incubated for further 24 h. Cell viability was then measured using MTT assay. Values are the average of six replicates and presented as the mean  $\pm$  S.D.  $\text{DL}_{50} = 9.2$  or 2.8  $\text{J}/\text{cm}^2$  at 0.1 and 1  $\mu\text{M}$  of TPC in NP-TPC-ATWLPPR, respectively.

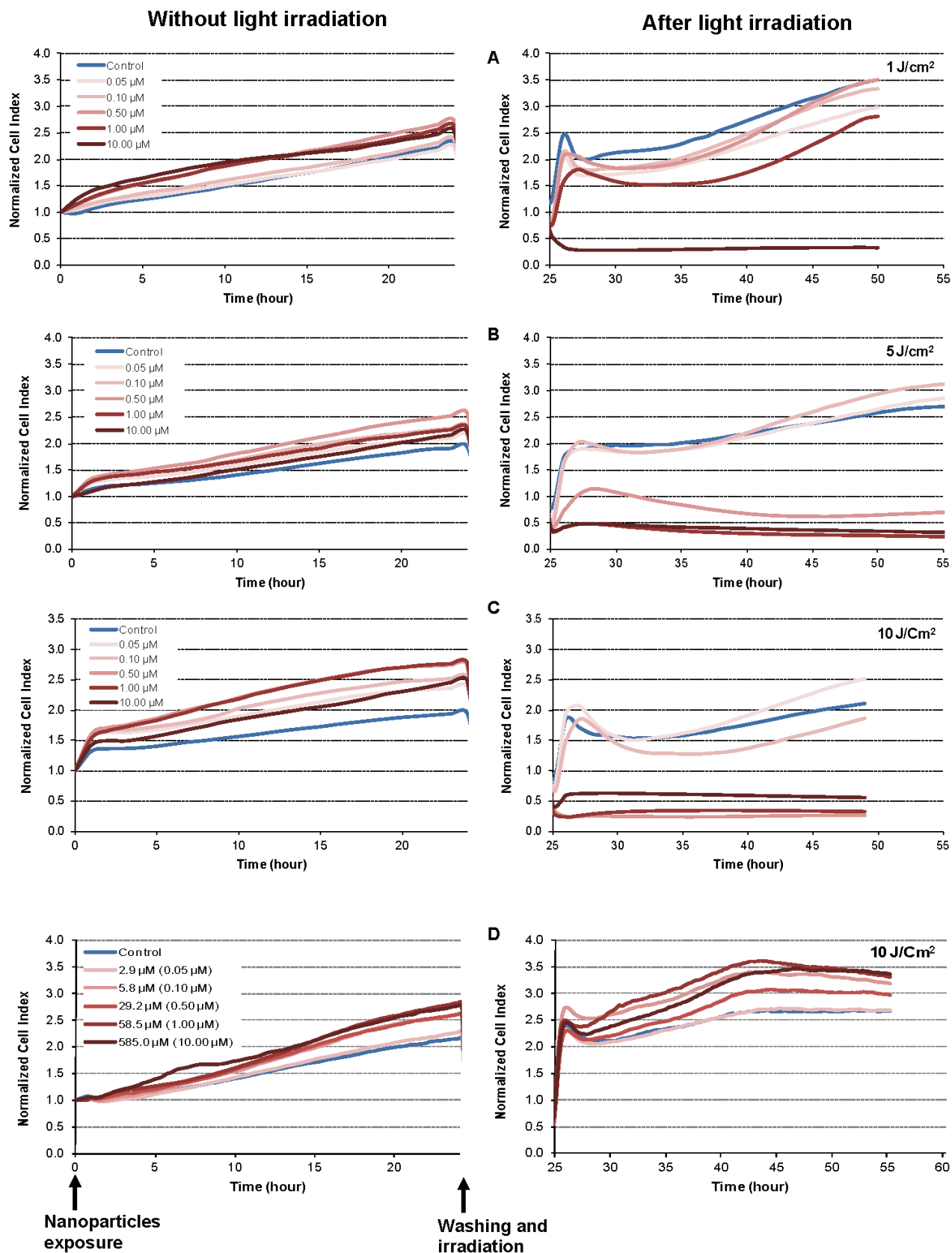


**Figure 5.** Kinetics of photo-induced cytotoxicity of nanoparticles according to real-time impedance-based analysis. MDA-MB-231 cells were monitored for 24 h during interaction with NP-TPC-ATWLPPR (A, B, C) or NP (D) at the indicated concentrations of photosensitizer or the corresponding concentration of gadolinium oxide for the control NP (left panel). Following washing, cells were exposed to various light doses (A: 1 J/cm<sup>2</sup>, B: 5 J/cm<sup>2</sup>, C and D: 10 J/cm<sup>2</sup>) (right panel). Presented cell index values are the mean of 6 replicates.

### Tumor tissue selectivity and MRI contrast enhancement *in vivo*

To investigate MRI contrast enhancement in tumor tissue, cerebral MRI analysis of *nude* rats with orthotopic U87 glioblastoma model was performed about 20 days after intracranial tumor implantation. MRI analysis of the tumor tissue was investigated for intravenously injected un-conjugated and peptide-targeted gadolinium-based hybrid nanoparticles. Dynamic data of MRI signal intensity from the selected regions of interest (ROIs) in the tumor and the controlateral tissue were expressed as the mean signal per area unit and used to create kinetics of MRI contrast enhancement (EHC %) for all time points post-injection. The kinetics represent MRI contrast

enhancement in both tumor and controlateral tissue normalized to the pre-injection MRI signal, and MRI contrast enhancement in tumor tissue normalized to controlateral tissue (Fig. 6A-B). As shown in Fig. 6A-B, immediately after intravenous injection, whatever the nanoparticles types the MRI contrast enhancement increased rapidly and specifically in tumor ROIs to achieve maximum enhancement at 2-7 min post-injection, reflecting nanoparticles incorporation in tumor. We can note that tumor MRI signal intensity appears to be higher in rats injected with non-targeted nanoparticles probably due to higher pre-injection MRI signal (2.5-fold) because of more extended tumor mass as compared to that injected with targeted nanoparticles (Fig. 6B-C).

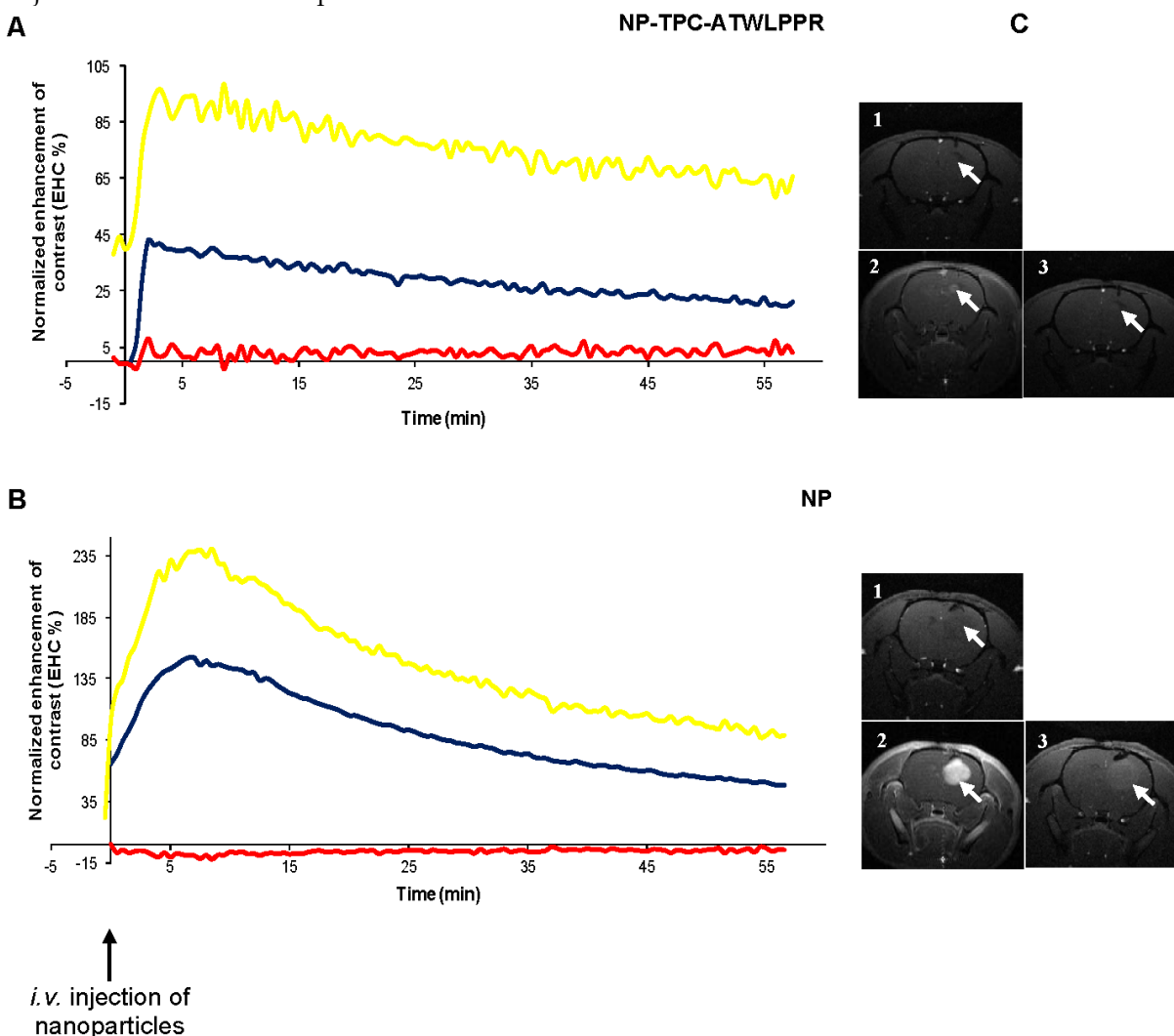


**Figure 6.** Cerebral biodistribution and tumor MRI contrast enhancement by gadolinium-based hybrid silica nanoparticles with or without targeting peptide monitored during 1h and, immediately after intravenous injection. Dynamic T1-weighted images acquisition was started before intravenous injection of the nanoparticles (25 μmol of Gd / 250 g of body weight) to characterize the kinetics of the nanoparticles biodistribution in the tumor. MRI signal intensity kinetics of injected peptide-conjugated NP-TPC-ATWLPPR (A), and un-conjugated NP (B) nanoparticles were expressed as the enhancement of contrast (EHC %) normalized on pre-injection signal. The curves represent time-dependent signal intensity recorded from different ROIs selected from: ■ Controlateral healthy hemisphere, ■ Tumor tissue, or ■ the EHC in the tumor tissue as normalized on the controlateral healthy hemisphere. C) T1 coronal MRI images obtained (1) before nanoparticles injection, (2) maximal MRI signal intensity after injection and (3) 1h post-injection.

Most interestingly however, distinct decrease rates of tumor MRI contrast kinetics from the maximum peak were observed according to nanoparticles type. Indeed, peptide-targeted nanoparticles showed slower time-dependent decrease (2.75-fold) of tumor MRI contrast as compared to non-targeted NP ( $-0.0072$  vs.  $-0.0198 \text{ min}^{-1}$ ). Using the semi-logarithmic presentation of MRI contrast enhancement decrease kinetics (data not shown), half-life of peptide-targeted nanoparticles in the tumor tissue was estimated to be 2.75-fold than that of the non-targeted nanoparticles

( $T_{1/2} = 96.25$  vs.  $35.00$  min). To evaluate *in vivo* biodistribution of the nanoparticles  $\sim 75$  min post-intravenous injection, tumor-bearing rats were sacrificed at the end of MRI analysis and organs were subjected to gadolinium content quantification. Post-mortem ICP-MS analysis of the organs/tissues showed that whatever the nanoparticles groups gadolinium was detected in liver at low levels, but essentially present in kidneys and urine (Fig. 7), suggesting rapid clearance of the nanoparticles by the renal route.

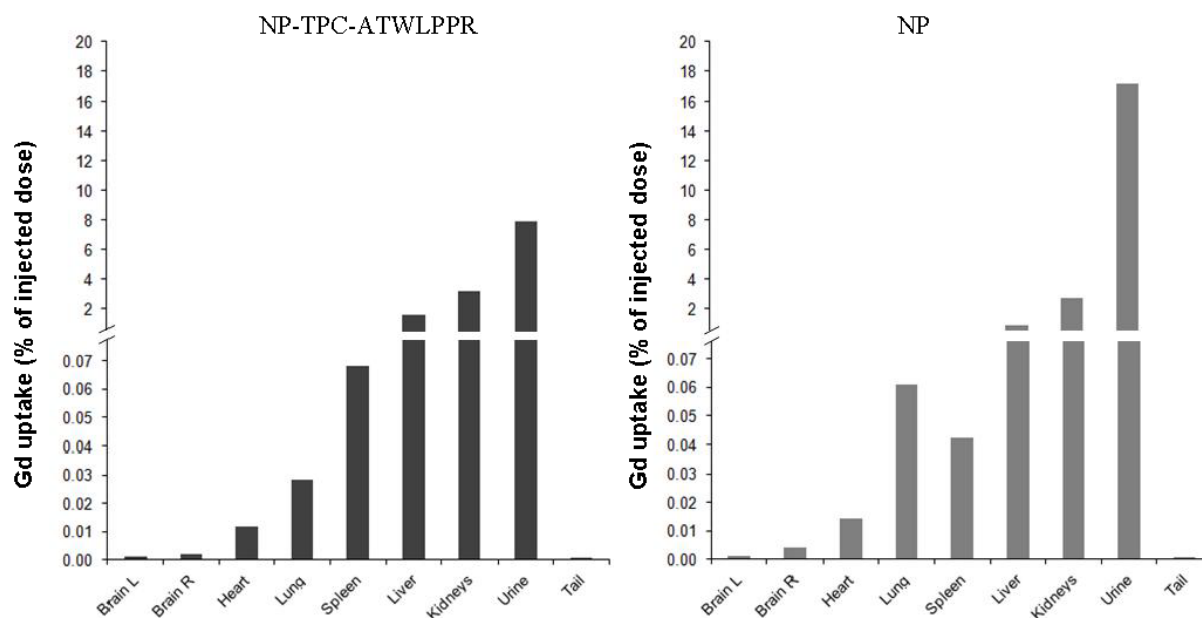


**Figure 7.** Biodistribution of gadolinium-based hybrid silica nanoparticles with or without targeting peptide at 1h15 after intravenous injection (25  $\mu\text{mol}$  of Gd/  $\sim 250$  g of body weight) in the caudal vein with NP-TPC-ATWLPPR (A) or NP (B). Gadolinium uptake was determined by ICP-MS analysis and expressed as percentage of the injected dose. Brain L: left brain hemisphere, Brain R: right brain hemisphere bearing xenografted tumor.

## Discussion

Our strategy aims to favor the vascular effect of PDT by targeting tumor-associated vascularisation using peptide-functionalized theranostic nanoparticles. The present study describes the development and the evaluation of novel small multifunctional silica-based nanoparticles as potential theranostic system for an integrated vascular-targeted PDT and MRI. Previous works of our group described the conjugation of chlorin photosensitizer to ATWLPPR peptide targeting NRP-1 over-expressed in tumor angiogenic vessels. In the present work, we developed ATWLPPR-targeted silica-based nanoparticles with gadolinium chelates as MRI contrast agent and a chlorin as photosensitizer. The nanoparticles were surface-functionalized with hydrophilic DOTAGA in part as scaffold for grafting of ATWLPPR peptide units. *In vitro* studies demonstrated the photodynamic

efficiency of the chlorine-doped multifunctional nanoparticles on cancer cells and their ability to target NRP-1 protein through the targeting peptide moiety.

Multifunctional nanoparticles demonstrated *in vitro* photodynamic efficiency related to photosensitizer concentration and light dose as showed by using both impedance-based real-time cell analysis and MTT assay. In the absence of light irradiation, our multifunctional nanoparticles displayed no cytotoxicity at low concentrations, except a delayed alteration of cell proliferation observed with the cell index kinetics. Such late effect may be due to long retention of nanoparticles in *in vitro* cell culture system. Indeed, we observed alterations in cell proliferation even for low concentrations of nanoparticles however MTT test only showed a cytotoxic effect with the highest test concentration of  $10 \mu\text{M}$ . This discrepancy already reported in the literature, may be mainly due to the fact that both assays measure distinct cell activities;

MTT test detects cell viability through mitochondrial metabolism, while RTCA considers cell death or proliferation, cell morphology, and cell adhesion to the well as defined by cells-microelectrode contact surface [42, 45-48]. This observation raises the question about the underlying mechanism of nanoparticles interaction on cellular activities. Numerous research groups have pointed out the difficulty of using classical single-point techniques usually based on cell metabolism activity to assess nanoparticles-related cytotoxicity [49, 50]. Multifunctional nanoparticles conferred photosensitivity to cancer cells, providing evidence that the photosensitizer molecules covalently grafted within the nanoparticle matrix can be photoactivated *in vitro*. As reported by our group [34], such nanoparticles indeed did not alter the photophysical properties of the encapsulated chlorin photosensitizer. Their photodynamic activity resulted in the loss of cell activities related to photosensitizer concentration and light dose since no photocytotoxicity was detected with control nanoparticles without photosensitizer. Accordingly, nanoparticles-encapsulated photosensitizer molecules inducing photosensitivity to cells were largely reported. Kopelman *et al.* synthesized a polyacrylamide multifunctional platform containing a MRI contrast enhancement agent and Photofrin® photosensitizer, as well as targeting unit (the integrin-targeting RGD peptide) for specific cell targeting [25, 51, 52]. *In vitro* studies confirmed the photoactivation of the encapsulated photosensitizer generating efficient PDT activity on cancer cells. More recently, Zhao *et al.*, described the synthesis of silica-coated lanthanide-doped nanoparticles with phthalocyanine (AIC4Pc) photosensitizer covalently incorporated inside the silica shell for PDT and MRI. The authors demonstrated the ability of the nanoparticles to kill cancer cell upon near-infrared irradiation without cytotoxicity in darkness [27].

Molecular affinity was investigated for peptide-functionalized nanoparticles, demonstrating the ability of ATWLPPR homing peptide to bind recombinant NRP-1 protein. Peptide-conjugated chlorin demonstrated a molecular affinity of 213  $\mu\text{M}$  ( $\text{EC}_{50}$  value, the concentration of competitor that displaced 50% of VEGF<sub>165</sub> binding) [38], ATWLPPR-targeted nanoparticles (~3 peptides per nanoparticle) showed a 3.5-fold high molecular recognition for NRP-1 protein ( $\text{EC}_{50}$  = 56.6  $\mu\text{M}$ ). This may be explained by a positive cooperativity in binding of nanoparticle-grafted ATWLPPR units through multivalent interactions with NRP-1 protein. Moreover, it is noticeable that previous findings of our group have still showed no additional increase of affinity with more than four peptides per nanoparticles [34] probably because ster-

ic hindrance due to the number of peptide units.

Real-time monitoring of *in vivo* MRI signal allowed us to demonstrate that intravenously injected nanoparticles induced specific enhancement of MRI contrast in tumor tissue, reflecting their high tumortropic accumulation. This reveals the potential of the nanoparticles as MRI contrast enhancer and suggests nanoparticles passive targeting of tumor tissue probably through the Enhanced Permeability and Retention (EPR) effect characterizing malignant tissues [53, 54]. Leaky vessels with large fenestrations result in extravasation and extensive leakage of circulating nanoparticles into the tumor tissue [17]. Slow venous return in tumor tissue and the poor lymphatic clearance cause intratumoral retention of nanoparticles. Furthermore, both types of nanoparticles are surface-functionalized with hydrophilic DOTAGA chelates that could endow the nanoparticles with water dispersibility and bioavailability [55] and improve their relaxivity properties [56, 55, 33]. Lux and co-workers (2011) have recently reported that similar small gadolinium hybrid nanoparticles functionalized with DOTA displayed significant increase of longitudinal relaxivities in solution with better MRI contrast enhancement *in vivo* as compared to DOTA(Gd) or DOTAREM®, among the most frequently used MRI contrast agents [33]. It should be noted that tumor MRI signal intensity appears to be higher with non-targeted nanoparticles probably due to the more extended tumor mass. Interestingly, we evidenced that ATWLPPR-targeted nanoparticles can favour the intratumoral retention of functionalized nanoparticles compared to control nanoparticles, providing a prolonged selective and positive MRI contrast enhancement. This could indicate that tumor clearance of peptide-targeted nanoparticles is delayed through peptide functionalization. Although the use of targeted nanoparticles as platforms for theranostic applications have been widely described, it is the first time that multifunctional silica-based nanoparticles targeting NRP-1 have been evaluated *in vivo* as a delivery system for PDT and imaging agents.

In this targeting strategy, we revealed the *in vitro* photodynamic efficiency of the multifunctional silica-based nanoparticles for PDT and their accumulation in tumor tissues. Our findings are promising and warrant further studies using these multifunctional nanoparticles for cancer theranostics *in vivo*.

## Abbreviations

APTES: AminoPropylTriEthoxySilane; ATCC: American Type Culture Collection; ATWLPPR: H-Ala-Thr-Trp-Leu-Pro-Pro-Arg-OH; Boc: *Tert*-butoxy carbonyl; BSA: Bovine Serum Albumine; CI: Cell

Index; DEG: diethylene glycol; DIEA: N,N-Diisopropylethylamine; DMF: Dimethylformamide; DMSO: Dimethyl sulfoxide; DOTAGA: (1,4,7,10-tetraazacyclododecane-1-glutaric anhydride-4,7,10-triacetic) acid; EDC: Ethylene DiChloride; EHC: Enhancement of Contrast; FBS: Fetal Bovine Serum; Fmoc: 9-fluorenyl-methoxy-carbonyl; HBSS: Hank's Buffered Salt Solution; HBTU: 2-(1*H*-benzotriazol-1-yl)-1,1,3,3-tetramethyl-uronium hexafluorophosphate; ICP-MS: Inductively coupled plasma-mass spectrometry; MRI: Magnetic Resonance Imaging; MTT: 3-(4,5-dimethylthiazol-2-yl)-2,5-diphenyl tetrazolium bromide; NP: Nanoparticle; NRP-1: Neuropilin-1 receptor; <sup>1</sup>O<sub>2</sub>: singlet oxygen; Pbf: 2,2,4,6,7-pentamethyldihydro-benzofuran-5-sulfonyl; PBS: Phosphate Buffered Saline; PCS: Photon Correlation Spectroscopy; PDT: photodynamic therapy; ROS: Reactive Oxygen Species; RPMI: Roswell Park Memorial Institute medium; RTCA SP: Real Time Cell Analyzer Single Plate; tBu: *tertio*-butyl; TEA: TriEthylAmine; TFA: trifluoroacetic acid; TEOS: TriEthOxy Silane; TPC: 5-(4-carboxyphenyl)-10,15,20-triphenylchlorin; TPC-NHS: 5,10,15,tri-(*p*-tolyl)-20-(*p*-carboxylphenyl)chlorinsuccinidyl ester; VEGF: Vascular Endothelial Growth Factor.

## Acknowledgment

This work was supported by the research funds of the French Ligue Nationale Contre le Cancer and the French ANR (Agence Nationale de la Recherche) project no. 08-PCV1-0021-01-entitled "NanoVTP". The funders had no role in study design, data collection and analysis, decision to publish, or preparation of the manuscript.

## Competing Interests

The authors have declared that no competing interest exists.

## References

- Weishaupt KR, Gomer CJ, Dougherty TJ. Identification of singlet oxygen as the cytotoxic agent in photoinactivation of a murine tumor. *Cancer Res.* 1976; 36: 2326-9.
- Fingar VH. Vascular effects of photodynamic therapy. *J Clin Laser Med Surg.* 1996; 14:323-8.
- Dougherty TJ, Gomer CJ, Henderson BW, Jori G, Kessel D, Korbelik M et al. Photodynamic therapy. *J Natl Cancer Inst.* 1998; 90: 889-905.
- Bonnett R. Photosensitizers of the porphyrin and phthalocyanine series for photodynamic therapy. *Chem Soc Rev.* 1995; 24: 19-33.
- McCaughan JS Jr. Photodynamic therapy: a review. *Drugs Aging.* 1999; 15: 49-68.
- Del Governatore M, Hamblin MR, Shea CR, Rizvi I, Molpus KG, Tanabe KK et al. Experimental photoimmunotherapy of hepatic metastases of colorectal cancer with a 17.1A chlorin(e6) immunoconjugate. *Cancer Res.* 2000; 60: 4200-5.
- Chaloin L, Bigey P, Loup C, Marin M, Galeotti N, Piechaczyk M et al. Improvement of porphyrin cellular delivery and activity by conjugation to a carrier peptide. *Bioconjug Chem.* 2001; 12: 691-700.
- Sharman WM, van Lier JE, Allen CM. Targeted photodynamic therapy via receptor mediated delivery systems. *Adv Drug Deliv Rev.* 2004; 56: 53-76.
- Tang W, Xu H, Kopelman R, Philbert MA. Photodynamic characterization and in vitro application of methylene blue-containing nanoparticle platforms. *Photochem Photobiol.* 2005; 81: 242-9.
- Konan YN, Berton M, Gurny R, Allémann E. Enhanced photodynamic activity of meso-tetra(4-hydroxyphenyl)porphyrin by incorporation into sub-200 nm nanoparticles. *Eur J Pharm Sci.* 2003; 18: 241-9.
- Qin M, Hah HJ, Kim G, Nie G, Lee YE, Kopelman R. Methylene blue covalently loaded polyacrylamide nanoparticles for enhanced tumor-targeted photodynamic therapy. *Photochem Photobiol Sci.* 2011; 10: 832-41.
- Tozer GM, Bicknell R. Therapeutic targeting of the tumor vasculature. *Semin Radiat Oncol.* 2004; 14: 222-32.
- Chen B, Pogue BW, Luna JM, Hardman RL, Hoopes PJ, Hasan T. Tumor vascular permeabilization by vascular-targeting photosensitization: effects, mechanism, and therapeutic implications. *Clin Cancer Res.* 2006; 12: 917-23.
- Folkman J. Angiogenesis in cancer, vascular, rheumatoid and other disease. *Nat Med.* 1995; 1: 27-31.
- Ichikawa K, Hikita T, Maeda N, Yonezawa S, Takeuchi Y, Asai T et al. Antiangiogenic photodynamic therapy (PDT) by using long-circulating liposomes modified with peptide specific to angiogenic vessels. *Biochim Biophys Acta.* 2005; 1669: 69-74.
- Fingar VH, Taber SW, Haydon PS, Harrison LT, Kempf SJ, Wieman TJ. Vascular damage after photodynamic therapy of solid tumors: a view and comparison of effect in pre-clinical and clinical models at the University of Louisville. *In Vivo.* 2000; 14: 93-100.
- Iyer AK, Khaled G, Fang J, Maeda H. Exploiting the enhanced permeability and retention effect for tumor targeting. *Drug Discov Today.* 2006; 11: 812-8.
- Starzec A, Ladam P, Vassy R, Badache S, Bouchemal N, Navaza A et al. Structure-function analysis of the antiangiogenic ATWLPPR peptide inhibiting VEGF(165) binding to neuropilin-1 and molecular dynamics simulations of the ATWLPPR/neuropilin-1 complex. *Peptides.* 2007; 28: 2397-402.
- Tirand L, Frochot C, Vanderesse R, Thomas N, Trinquet E, Pinel S et al. A peptide competing with VEGF165 binding to neuropilin-1 mediates targeting of a chlorin-type photosensitizer and potentiates its photodynamic activity in human endothelial cells. *J Control Release.* 2006; 111: 153-64.
- Thomas N, Bechet D, Becuwe P, Tirand L, Vanderesse R, Frochot C et al. Peptide-conjugated chlorin-type photosensitizer binds neuropilin-1 in vitro and in vivo. *J Photochem Photobiol B.* 2009; 96: 101-8.
- Thomas N, Tirand L, Chatelut E, Plénat F, Frochot C, Dodeller M et al. Tissue distribution and pharmacokinetics of an ATWLPPR-conjugated chlorin-type photosensitizer targeting neuropilin-1 in glioma-bearing nude mice. *Photochem Photobiol Sci.* 2008; 7: 433-41.
- Bechet D, Tirand L, Faivre B, Plénat F, Bonnet C, Bastogne T et al. Neuropilin-1 targeting photosensitization-induced early stages of thrombosis via tissue factor release. *Pharm Res.* 2010; 27: 468-79.
- Tirand L, Thomas N, Dodeller M, Dumas D, Frochot C, Maunin B et al. Metabolic profile of a peptide-conjugated chlorin-type photosensitizer targeting neuropilin-1: an in vivo and in vitro study. *Drug Metab Dispos.* 2007; 35: 806-13.
- Chatterjee DK, Fong LS, Zhang Y. Nanoparticles in photodynamic therapy: an emerging paradigm. *Adv Drug Deliv Rev.* 2008; 60: 1627-37.
- Kopelmana R, Koo YEL, Philbert M, Moffat BA, Reddy GR, McConville P et al. Multifunctional nanoparticle platforms for in vivo MRI enhancement and photodynamic therapy of a rat brain cancer. *Journal of Magnetism and Magnetic Materials.* 2005; 293: 404-10.
- Reddy GR, Bhojani MS, McConville P, Moody J, Moffat BA, Hall DE et al. Vascular targeted nanoparticles for imaging and treatment of brain tumors. *Clin Cancer Res.* 2006; 12: 6677-86.
- Zhao Z, Han Y, Lin C, Hu D, Wang F, Chen X et al. Multifunctional core-shell upconverting nanoparticles for imaging and photodynamic therapy of liver cancer cells. *Chem Asian J.* 2012; 7: 830-7.
- Lee SJ, Park K, Oh YK, Kwon SH, Her S, Kim IS et al. Tumor specificity and therapeutic efficacy of photosensitizer-encapsulated glycol chitosan-based nanoparticles in tumor-bearing mice. *Biomaterials.* 2009; 30: 2929-39.
- Bechet D, Couleaud P, Frochot C, Viriot ML, Guillemin F, Barberi-Heyob M. Nanoparticles as vehicles for delivery of photodynamic therapy agents. *Trends Biotechnol.* 2008; 26: 612-21.

30. Brevet D, Gary-Bobo M, Raehm L, Richeter S, Hocine O, Amro K, Loock B et al. Mannose-targeted mesoporous silica nanoparticles for photodynamic therapy. *Chem Commun (Camb)*. 2009; (12): 1475-7.
31. Bridot JL, Faure AC, Laurent S, Rivière C, Billotey C, Hiba B et al. Hybrid gadolinium oxide nanoparticles: multimodal contrast agents for in vivo imaging. *J Am Chem Soc*. 2007; 129: 5076-84.
32. Faure AC, Dufort S, Josserand V, Perriat P, Coll JL, Roux S et al. Control of the in vivo biodistribution of hybrid nanoparticles with different poly(ethylene glycol) coatings. *Small*. 2009; 5: 2565-75.
33. Lux F, Mignot A, Mowat P, Louis C, Dufort S, Bernhard C et al. Ultrasmall rigid particles as multimodal probes for medical applications. *Angew Chem Int Ed Engl*. 2011; 50: 12299-303.
34. Couleaud P, Bechet D, Vanderesse R, Barberi-Heyob M, Faure AC, Roux S et al. Functionalized silica-based nanoparticles for photodynamic therapy. *Nanomedicine (Lond)*. 2011; 6: 995-1009.
35. Bazzi R, Flores-Gonzalez MA, Louis C, Lebbou K, Dujardin C, Brenier A, et al. Synthesis and uminescent properties of sub-5-nm lanthanide oxides nanoparticles. *Journal of Luminescence*. 2003; 102: 445-50
36. Bazzi R, Flores MA, Louis C, Lebbou K, Zhang W, Dujardin C et al. Synthesis and properties of europium-based phosphors on the nanometer scale: Eu<sub>2</sub>O<sub>3</sub>, Gd<sub>2</sub>O<sub>3</sub>:Eu, and Y<sub>2</sub>O<sub>3</sub>:Eu. *J Colloid Interface Sci*. 2004; 273: 191-7.
37. Louis C, Bazzi R, Marquette CA, Bridot JL, Roux S, Ledoux G et al. Nanosized hybrid particles with double luminescence for biological labelling. *Chem Mater*. 2005; 17: 1673-82.
38. Thomas N, Pernot M, Vanderesse R, Becuwe P, Kamarulzaman E, Da Silva D et al. Photodynamic therapy targeting neuropilin-1: Interest of pseudopeptides with improved stability properties. *Biochem Pharmacol*. 2010; 80: 226-35.
39. Whitlock Jr HW, Hanauer R, Oester MY, Bower BK. Diimid reduction of porphyrins. *J Am Chem Soc*. 1969; 91: 7485-9.
40. Di Stasio B, Frochot C, Dumas D, Even P, Zwier J, Müller A et al. The 2-aminoglucosamide motif improves cellular uptake and photodynamic activity of tetraphenylporphyrin. *Eur J Med Chem*. 2005; 40: 1111-22.
41. Tanford C. *Physical Chemistry of Macromolecules*. John Wiley and Sons: New York; 1961.
42. Kirstein SL, Atienza JM, Xi B, Zhu J, Yu N, Wang X et al. Live cell quality control and utility of real-time cell electronic sensing for assay development. *Assay Drug Dev Technol*. 2006; 4: 545-53.
43. Urcan E, Haertel U, Styllou M, Hickel R, Scherthan H, Reichl FX. Real-time xCELLigence impedance analysis of the cytotoxicity of dental composite components on human gingival fibroblasts. *Dent Mater*. 2010; 26: 51-8.
44. Schneider R, Schmitt F, Frochot C, Fort Y, Lourette N, Guillemin F et al. Design, synthesis, and biological evaluation of folic acid targeted tetraphenylporphyrin as novel photosensitizers for selective photodynamic therapy. *Bioorg Med Chem*. 2005; 13: 2799-808.
45. Quereda JJ, Martínez-Alarcón L, Mendoca L, Majado MJ, Herro-Medrano JM, Pallarés FJ et al. Validation of xCELLigence real-time cell analyzer to assess compatibility in xenotransplantation with pig-to-baboon model. *Transplant Proc*. 2010; 42: 3239-43.
46. Heng BC, Das GK, Zhao X, Ma LL, Tan TT, Ng KW et al. Comparative cytotoxicity evaluation of lanthanide nanomaterials on mouse and human cell lines with metabolic and DNA-quantification assays. *Biointerphases*. 2010; 5: FA88-97.
47. Soenen SJ, De Cuyper M. Assessing cytotoxicity of (iron oxide-based) nanoparticles: an overview of different methods exemplified with cationic magnetoliposomes. *Contrast Media Mol Imaging*. 2009; 4: 207-19.
48. Hanusová V, Králová V, Schröterová L, Trilecová L, Pakostová A, Skálová L. The effectiveness of oracin in enhancing the cytotoxicity of doxorubicin through the inhibition of doxorubicin deactivation in breast cancer MCF7 cells. *Xenobiotica*. 2010; 40: 681-90.
49. Soenen SJ, Rivera-Gil P, Montenegro JM, Parak WJ, De Smedt SC, Kevin Braeckmans. Cellular toxicity of inorganic nanoparticles: Common aspects and guidelines for improved nanotoxicity evaluation. *Nano Today*. 2011; 6: 446-65
50. Mariani V, Ponti J, Giudetti G, Broggi F, Marmorato P, Gioria S et al. Online monitoring of cell metabolism to assess the toxicity of nanoparticles: the case of cobalt ferrite. *Nanotoxicology*. 2012; 6: 272-87.
51. Ross B, Rehemtulla A, Koo YEL, Reddy R, Kim G, Behrend C et al. Photonic and Magnetic Nanoexplorers for Biomedical Use: From Sub-cellular Imaging to Cancer Diagnostics and Therapy. *Proc SPIE-Int Soc Optical Eng*. 2004; :76-83.
52. Koo YE, Fan W, Hah H, Xu H, Orringer D, Ross B et al. Photonic explorers based on multifunctional nanoplatfoms for biosensing and photodynamic therapy. *Appl Opt*. 2007; 46: 1924-30.
53. Khemtong C, Kessinger CW, Gao J. Polymeric nanomedicine for cancer MR imaging and drug delivery. *Chem Commun (Camb)*. 2009; (24): 3497-510.
54. Barreto JA, O'Malley W, Kubeil M, Graham B, Stephan H, Spiccia L. Nanomaterials: applications in cancer imaging and therapy. *Adv Mater*. 2011; 23: H18-40.
55. Liu T, Li X, Qian Y, Hu X, Liu S. Multifunctional pH-disintegrable micellar nanoparticles of asymmetrically functionalized  $\beta$ -cyclodextrin-based star copolymer covalently conjugated with doxorubicin and DOTA-Gd moieties. *Biomaterials*. 2012; 33: 2521-31.
56. Ratzinger G, Agrawal P, Körner W, Lonkai J, Sanders HM, Terreno E et al. Surface modification of PLGA nanospheres with Gd-DTPA and Gd-DOTA for high-relaxivity MRI contrast agents. *Biomaterials*. 2010; 31: 8716-23.